

Stochastic Voronoi Ensembles for Anomaly Detection

Yang Cao^{1,2}

Abstract

Anomaly detection aims to identify data instances that deviate significantly from majority of data, which has been widely used in fraud detection, network security, and industrial quality control. Existing methods struggle with datasets exhibiting varying local densities: distance-based methods miss local anomalies, while density-based approaches require careful parameter selection and incur quadratic time complexity. We observe that local anomalies, though indistinguishable under global analysis, become conspicuous when the data space is decomposed into restricted regions and each region is examined independently. Leveraging this geometric insight, we propose SVEAD (Stochastic Voronoi Ensembles Anomaly Detector), which constructs ensemble random Voronoi diagrams and scores points by normalized cell-relative distances weighted by local scale. The proposed method achieves linear time complexity and constant space complexity. Experiments on 45 datasets demonstrate that SVEAD outperforms 12 state-of-the-art approaches.

1. Introduction

Anomaly detection is the task of identifying instances that deviate significantly from the majority of data, has been a fundamental problem in machine learning with applications spanning fraud detection, network security, medical diagnosis, and industrial quality control (Chandola et al., 2009; Liu et al., 2024; Cao et al., 2024a;c). The central challenge lies in distinguishing outliers from natural variations when data exhibits heterogeneous structures, multiple clusters, or varying densities.

Existing detection strategies face complementary limitations. Distance-based methods (Angiulli & Pizzuti, 2002) efficiently identify global outliers but fail to detect anomalies in regions with varying local densities, as they apply

¹Tsinghua Shenzhen International Graduate School, China.

²Great Bay University, China.. Correspondence to: Yang Cao <charles.cao@ieee.org>.

Preprint. January 8, 2026.

uniform distance thresholds across the entire feature space without adapting to local data concentration. Density-based approaches (Breunig et al., 2000) address this by measuring local data density to capture local anomalies, but introduce quadratic computational costs and sensitivity to neighborhood parameters. Recent deep learning methods employ autoencoders or generative models to capture complex patterns through reconstruction error or likelihood estimation, yet require substantial training overhead and careful hyper-parameter tuning (Pang et al., 2021).



(a) Original Painting.



(b) Isolation Distributional Kernel.



(c) SVEAD.

Figure 1. Demonstration of anomaly score heatmap on *Lanting Xu* calligraphy pixel data. (a) Original image with black characters considered as anomalies. (b) Anomaly score Heatmap from IDK. (c) Anomaly score Heatmap from SVEAD.

These limitations suggest examining the problem from a geometric perspective, which reveals an overlooked property: **anomalies that appear indistinguishable under global analysis become conspicuous when examined within restricted spatial contexts**. By evaluating samples within dynamically defined spatial regions, we can identify both global and local anomalies through a unified scoring mecha-

nism.

Leveraging this geometric principle, we propose the Stochastic Voronoi Ensembles Anomaly Detector (SVEAD). The proposed algorithm constructs an ensemble of random space partitions via Voronoi diagram. Each partition is generated by randomly sampling a subset of data points as anchors, inducing a Voronoi decomposition where each point is assigned to its nearest anchor. Within each Voronoi cell, we measure how far a point lies from its anchor relative to other points in the same cell. Specifically, distances are normalized by the maximum distance within the cell and weighted by the mean distance, adapting to local scale variations. The final anomaly score is obtained by averaging across all partitions in the ensemble. The method achieves linear time complexity and constant space complexity.

To illustrate detection capability of SVEAD, Figure 1 shows results on a section from the classical Chinese calligraphy *Lanting Xu*, where black ink characters are treated as anomalies against the aged paper background. Compared to the state-of-the-art Isolation Distributional Kernel (IDK) (Ting et al., 2020; 2021), SVEAD produces significantly sharper anomaly score maps with clearer character boundaries and better background-foreground separation.

The choice of Voronoi diagram with random anchor sampling is motivated by three properties: **1) Data-dependent:** randomly sampling anchors naturally produces more anchors in dense regions and fewer in sparse regions, resulting in smaller cells where data is concentrated and larger cells where data is sparse. **2) High-efficiency:** Voronoi cells are defined purely by geometric proximity without requiring neighborhood size or distance threshold parameters. **3) Non-overlapping:** the diagram divides data space into non-overlapping cells where each point belongs to exactly one cell, ensuring each point receives an unambiguous anomaly score.

The key contributions of this work are:

- proposing SVEAD, an ensemble-based algorithm that leverages stochastic Voronoi diagrams to capture multi-scale anomaly patterns without explicit parameter learning or complex model architectures.
- introducing a dual-factor scoring mechanism that combines relative position normalization with local density weighting, which enables adaptive anomaly detection across varying density regions without explicit density estimation.
- demonstrating the ability SVEAD to detect different types of anomalies, including global, local and dependency anomaly.
- conducting extensive experiments on 45 datasets showing that SVEAD achieves state-of-the-art performance while maintaining computational efficiency and inter-

preability.

2. Problem Formulation

Anomaly Detection Task. Consider a dataset $\mathcal{X} = \{\mathbf{x}_1, \mathbf{x}_2, \dots, \mathbf{x}_n\}$ where each instance $\mathbf{x}_i \in \mathbb{R}^d$ is represented by d features. The objective of anomaly detection is to learn a scoring function $f : \mathbb{R}^d \rightarrow \mathbb{R}$ that assigns higher scores to anomalous instances and lower scores to normal instances.

Anomaly Types. Anomalies are normally categorized into three types(Han et al., 2022):

Global anomalies \mathbf{x}_g that are distant from all data points. Let $\rho(\mathbf{x})$ denote the local density at point \mathbf{x} . A global anomaly satisfies $\rho(\mathbf{x}_g) \ll \mathbb{E}_{\mathbf{x} \in \mathcal{X}}[\rho(\mathbf{x})]$, residing in sparse regions of the feature space with consistently low density across all scales.

Local anomalies \mathbf{x}_l that deviate within their neighborhood $\mathcal{N}(\mathbf{x}_l)$ despite appearing normal globally. Formally, $\rho(\mathbf{x}_l) < \mathbb{E}_{\mathbf{x} \in \mathcal{N}(\mathbf{x}_l)}[\rho(\mathbf{x})]$ while $\rho(\mathbf{x}_l) \approx \mathbb{E}_{\mathbf{x} \in \mathcal{X}}[\rho(\mathbf{x})]$. These anomalies exhibit unusual patterns relative to their local context but conform to global statistics.

Dependency anomalies \mathbf{x}_c where features violate the dependency structure of normal data. Normal data exhibit feature dependencies such that $p(\mathbf{x}) \neq \prod_{i=1}^d p(x_i)$, while dependency anomalies have independent features: $p(\mathbf{x}_c) \approx \prod_{i=1}^d p(x_{c,i})$. Each marginal distribution $p(x_{c,i})$ remains consistent with normal data, but the joint distribution lacks the correlations present in normal instances.

Unsupervised Setting. We focus on the unsupervised anomaly detection setting where \mathcal{X} contains an unknown mixture of normal instances (majority class) and anomalous instances (minority class). Let $\mathcal{X} = \mathcal{X}_{\text{normal}} \cup \mathcal{X}_{\text{anom}}$ where $|\mathcal{X}_{\text{anom}}| \ll |\mathcal{X}_{\text{normal}}|$. The detector must identify $\mathcal{X}_{\text{anom}}$ without access to labeled data, relying solely on the assumption that anomalies are rare and exhibit distributional differences from the majority. This contrasts with the semi-supervised one-class setting where $\mathcal{X} = \mathcal{X}_{\text{normal}}$ during training, providing a clean reference of normal behavior.

3. Related Work

Existing anomaly detection methods can be broadly categorized into shallow and deep learning-based methods (Han et al., 2022).

3.1. Shallow methods

Distance-based methods like k-NN (Ramaswamy et al., 2000) compute anomaly scores based on distances to nearest neighbors, but fail in datasets with varying densities,

where normal points in sparse regions are misclassified as anomalies due to large neighbor distances. Density-based approaches address this limitation by examining local density variations. LOF (Breunig et al., 2000) introduced the concept of local reachability density, comparing each point’s density to its neighbors’ densities through density ratios. Points with significantly lower local density are identified as anomalies. While LOF handles varying densities better than distance-based methods, it suffers from quadratic time complexity due to k-nearest neighbor computations and requires careful selection of the neighborhood parameter k .

Statistical methods take a different approach by modeling feature distributions. COPOD (Li et al., 2020) uses empirical copula-based modeling to capture feature dependencies while computing tail probabilities for anomaly scoring. ECOD (Li et al., 2022) simplifies this by using empirical cumulative distribution functions with feature independence assumptions, estimating tail probabilities for each dimension and aggregating them into anomaly scores. These methods identify points in low-probability regions as anomalies.

Isolation-based methods fundamentally differ from density profiling approaches. Instead of characterizing normal behavior, they exploit the principle that anomalies are easier to isolate. Isolation Forest (Liu et al., 2008) constructs an ensemble of random trees that partition data through recursive axis-aligned splits. Anomalies require fewer partitions to isolate, resulting in shorter path lengths. The method provides linear time complexity and parameter-free operation but struggles with local anomalies in dense regions due to its axis-aligned partitioning bias. Recent isolation variants address local anomaly detection. iNNE (Bandaragoda et al., 2018) replaces axis-aligned splits with hypersphere-based partitioning, where each hypersphere is centered at a randomly sampled point with radius determined by the nearest neighbor distance. IDK (Ting et al., 2020; 2021) further advances this direction by employing data-dependent kernels and kernel mean embeddings to measure distributional similarities (Cao et al., 2025a), which has also been used for time series (Ting et al., 2024; Cao et al., 2024d), streaming (Cao et al., 2024b; Xu et al., 2025) and text (Cao et al., 2025b) anomaly detection.

3.2. Deep learning methods

Deep learning methods leverage neural networks to learn complex data representations for anomaly detection. Autoencoder-based approaches () learn to compress and reconstruct normal data, detecting anomalies through reconstruction error. The underlying assumption is that normal patterns lie on a low-dimensional manifold that the autoencoder learns, while anomalies deviate from this manifold and incur higher reconstruction loss.

One-class deep learning methods learn compact representa-

tions of normal data. DeepSVDD (Ruff et al., 2018) trains neural networks to map normal instances to a hypersphere with minimal volume in the learned feature space. Anomalies are identified as points falling outside or far from this hypersphere. Graph-based deep methods model relational structures in data. LUNAR (Goodge et al., 2022) employs graph neural networks to capture local neighborhood information, learning node representations that encode structural properties for anomaly detection.

Recent approaches combine deep learning with traditional techniques or introduce novel self-supervised paradigms. DIF (Xu et al., 2023a) uses neural networks for feature extraction and applies isolation forests on learned representations. SLAD (Xu et al., 2023b) introduces scale learning for tabular data, randomly sampling feature subspaces and learning to rank representations transformed from varied subspaces through distribution alignment. The method learns inherent data regularities without requiring explicit k-NN computations or density estimation. DTE (Livernoche et al., 2024) estimates the posterior distribution over diffusion timesteps for input samples to detect anomalies.

4. Methodology

Table 1. Summary of notation

Symbol	Description
\mathcal{X}	Dataset containing n data points
\mathbf{x}_i	The i -th data point, $\mathbf{x}_i \in \mathbb{R}^d$
n	Number of data points in dataset
d	Feature dimensionality
m	Number of anchors per partition
t	Ensemble size (number of partitions)
$\mathcal{A}^{(k)}$	Anchor set for the k -th partition
$a_i^{(k)}$	The i -th anchor in the k -th partition
$C_i^{(k)}$	Voronoi cell of anchor a_i in the k -th partition
$\mathcal{P}^{(k)}$	The k -th partition, $\mathcal{P}^{(k)} = \{C_1^{(k)}, \dots, C_m^{(k)}\}$
δ	Distance from point to its assigned anchor
δ_{\max}	Maximum distance within a Voronoi cell
δ_{mean}	Mean distance within a Voronoi cell
$s^{(k)}(\mathbf{x})$	Anomaly score of \mathbf{x} in the k -th partition
$f(\mathbf{x})$	Final anomaly score of \mathbf{x} (ensemble average)
$\rho(\mathbf{x})$	Local density at point \mathbf{x}
$\mathcal{N}(\mathbf{x})$	Neighborhood of point \mathbf{x}
τ	Anomaly detection threshold

In this section, we introduce SVEAD (Stochastic Voronoi Ensemble Anomaly Detector), a geometric approach to anomaly detection that leverages random space partitioning through Voronoi diagrams. The core insight is that *anomalies reveal themselves through their positions within locally defined spatial regions: points residing far from local anchors, particularly in sparse cells, are more likely to*

be anomalous. Table 1 summarizes the key notation used throughout this paper.

SVEAD operates in three stages. First, we construct an ensemble of Voronoi diagrams by repeatedly sampling random subsets of data points as anchors. Each anchor set induces a partition where every point is assigned to its nearest anchor, creating a collection of Voronoi cells. Second, within each cell, we score points by combining their normalized distance to the anchor with the cell’s mean distance, yielding a measure that adapts to local density variations. Third, we aggregate scores across all partitions through ensemble averaging, producing robust anomaly assessments that capture both global and local deviations.

This design offers three key advantages. **1)** Random anchor sampling provides computational efficiency, requiring only nearest-anchor queries rather than complete diagram construction. **2)** Voronoi diagrams supplies density-adaptive partitioning, where cell sizes naturally reflect local data concentration. **3)** Ensemble averaging delivers robustness, allowing different random partitions to capture complementary local structures while mitigating sensitivity to any single partition.

4.1. Stochastic Voronoi diagrams via anchor sampling

We adopt a sampling-based approach that constructs implicit Voronoi diagrams efficiently, Figure 2 shows the anchor sampling and voronoi diagram ensembles.

Anchor Sampling. For each partition, we randomly sample m points from the dataset \mathcal{X} without replacement to form an anchor set $\mathcal{A} = \{a_1, a_2, \dots, a_m\}$ where $m \ll n$. These anchors serve as generators for the Voronoi diagrams. The sampling is performed uniformly, ensuring that dense regions naturally receive more anchors due to higher point concentration, while sparse regions receive fewer anchors. This automatic density adaptation occurs without explicit density estimation.

Voronoi Cell Assignment. Given anchor set \mathcal{A} , the Voronoi cell C_i associated with anchor a_i is defined as:

$$C_i = \{\mathbf{x} \in \mathcal{X} : \|\mathbf{x} - a_i\| \leq \|\mathbf{x} - a_j\|, \forall j \neq i\} \quad (1)$$

where $\|\cdot\|$ denotes the Euclidean distance. Each point $\mathbf{x} \in \mathcal{X}$ is assigned to its nearest anchor, creating a partition $\{C_1, C_2, \dots, C_m\}$ that satisfies two properties: (1) $\bigcup_{i=1}^m C_i = \mathcal{X}$, ensuring complete coverage, and (2) $C_i \cap C_j = \emptyset$ for $i \neq j$, ensuring exclusivity. Unlike explicit Voronoi diagram construction, we do not compute cell boundaries or vertices; we only determine point-to-cell membership through nearest-anchor queries.

Ensemble Construction. A single random partition may be unstable, as different anchor samples can produce vastly different cell configurations. To achieve robustness, we repeat

the sampling and partitioning process t times, generating an ensemble of diagrams $\{\mathcal{P}^{(1)}, \mathcal{P}^{(2)}, \dots, \mathcal{P}^{(t)}\}$ where each $\mathcal{P}^{(k)}, k \in 1 \dots t$ represents the k -th partition with its own anchor set $\mathcal{A}^{(k)}$ and cell assignment. Each partition provides an independent view of the data’s local structure. Points that consistently appear far from anchors across multiple partitions are more likely to be genuine anomalies, while random fluctuations in individual partitions are averaged out.

4.2. Anomaly Scoring Mechanism

The scoring mechanism operates within each Voronoi cell, measuring how anomalous a point appears relative to its local context. A naive approach would directly use the distance to the nearest anchor, but this **fails to account for varying cell sizes and local density patterns**. We introduce a dual-factor scoring scheme that addresses these challenges.

Within-Cell Scoring. Consider a point $\mathbf{x} \in C_i$ assigned to anchor a_i in cell C_i . We define its anomaly score within this partition as:

$$s(\mathbf{x}) = \frac{\|\mathbf{x} - a_i\|}{\max_{\mathbf{x}' \in C_i} \|\mathbf{x}' - a_i\|} \cdot \frac{1}{|C_i|} \sum_{\mathbf{x}' \in C_i} \|\mathbf{x}' - a_i\| \quad (2)$$

where the first term δ/δ_{\max} normalizes the distance by the maximum cell radius, and the second term δ_{mean} represents the mean distance within the cell. We denote $\delta = \|\mathbf{x} - a_i\|$, $\delta_{\max} = \max_{\mathbf{x}' \in C_i} \|\mathbf{x}' - a_i\|$, and $\delta_{\text{mean}} = \frac{1}{|C_i|} \sum_{\mathbf{x}' \in C_i} \|\mathbf{x}' - a_i\|$, yielding the compact form from Equation 4.2:

$$s(\mathbf{x}) = \frac{\delta}{\delta_{\max}} \cdot \delta_{\text{mean}} \quad (3)$$

Rationale for Dual Factors. Each component serves a distinct purpose in anomaly assessment:

Relative position normalization (δ/δ_{\max}): This term measures where a point lies within its cell, producing values in $[0, 1]$. Without normalization, raw distances are incomparable across cells of different sizes. A point 10 units from its anchor in a large sparse cell may be more normal than a point 2 units away in a small dense cell. Normalization by δ_{\max} eliminates this scale dependency, treating each cell as a unit hypersphere where edge points receive scores near 1 regardless of absolute cell size.

Local density weighting (δ_{mean}): If we used only δ/δ_{\max} , we would implicitly assume that every cell should contribute equal numbers of anomalies. This is incorrect because cells in sparse regions naturally contain fewer normal points than cells in dense regions. The mean distance δ_{mean} serves as a proxy for inverse local density. In dense regions where

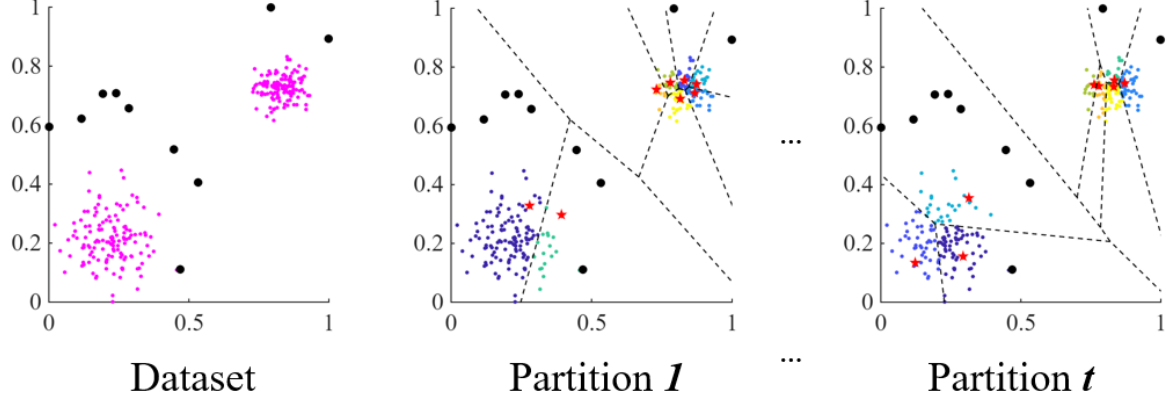


Figure 2. Illustration of SVEAD’s space partition and ensemble approach. Left: Original dataset with normal points (purple) and anomalies (black). Middle and Right: demonstration of two random partitions with different anchor sets (red stars). Each partition creates distinct Voronoi cells (dashed lines), assigning points to nearest anchors.

points cluster tightly around anchors, δ_{mean} is small, suppressing anomaly scores. In sparse regions where points spread widely, δ_{mean} is large, amplifying scores. This weighting ensures that points at cell edges in sparse regions receive higher scores than edge points in dense regions.

Connection to Density Estimation. The mean distance δ_{mean} naturally encodes local density information. Consider a Voronoi cell containing $|C_i|$ points distributed around anchor a_i . If these points occupy a volume V_i in feature space, the local density is approximately $\rho_i \propto |C_i|/V_i$. For a roughly spherical cell, the mean distance relates to volume through $V_i \propto \delta_{\text{mean}}^d$ where d is the dimensionality. Therefore:

$$\delta_{\text{mean}} \propto V_i^{1/d} \propto \left(\frac{|C_i|}{\rho_i} \right)^{1/d} \propto \rho_i^{-1/d} \quad (4)$$

Thus δ_{mean} increases as density decreases, providing an adaptive density estimator without explicit k-NN computations. The complete scoring function $(\delta/\delta_{\text{max}}) \cdot \delta_{\text{mean}}$ combines relative position with density adaptation, assigning high scores to points that are both far from their local anchor and located in sparse regions.

Ensemble Aggregation. Across t partitions, a point \mathbf{x} receives t scores $\{s^{(1)}(\mathbf{x}), s^{(2)}(\mathbf{x}), \dots, s^{(t)}(\mathbf{x})\}$. The final anomaly score is computed as the arithmetic mean:

$$f(\mathbf{x}) = \frac{1}{t} \sum_{k=1}^t s^{(k)}(\mathbf{x}) \quad (5)$$

Ensemble aggregation stabilizes scores by reducing variance introduced by random anchor sampling. Genuine anomalies consistently receive high scores across partitions because they remain distant from anchors and reside in sparse cells regardless of the specific anchor configuration. Normal points exhibit more variation, as some partitions may place

anchors nearby while others do not, but their averaged scores remain low due to overall proximity to the data distribution.

4.3. Theoretical Properties

We establish theoretical properties that explain why SVEAD effectively identifies anomalies through random Voronoi diagrams and ensemble averaging.

Density Adaptation Property. The expected cell size in random Voronoi diagrams naturally reflects local data density, providing automatic scale adaptation without explicit density estimation.

Proposition 4.1 (Cell Size and Density). *Consider a region $R \subset \mathbb{R}^d$ with local density $\rho(R)$. When uniformly sampling m anchors from dataset \mathcal{X} , the expected number of anchors falling in R is proportional to $\rho(R) \cdot |R|$, where $|R|$ denotes the volume of R . Consequently, the expected Voronoi cell size in R is inversely proportional to $\rho(R)$.*

Proof. Let N_R denote the number of data points in region R , and let M_R denote the number of anchors falling in R . Under uniform sampling, the probability that any sampled anchor falls in R is $p_R = N_R/n$. The expected number of anchors in R is:

$$\mathbb{E}[M_R] = m \cdot p_R = m \cdot \frac{N_R}{n} \quad (6)$$

Since $N_R \approx \rho(R) \cdot |R|$ for sufficiently large N_R , we have:

$$\mathbb{E}[M_R] \propto \rho(R) \cdot |R| \quad (7)$$

The expected cell size in R is the volume divided by the number of anchors:

$$\mathbb{E}[\text{cell size in } R] \approx \frac{|R|}{\mathbb{E}[M_R]} \propto \frac{1}{\rho(R)} \quad (8)$$

Thus, higher density regions produce smaller cells, and lower density regions produce larger cells. \square

This property ensures that δ_{mean} serves as a valid density proxy: in dense regions, smaller cells yield smaller δ_{mean} , while in sparse regions, larger cells yield larger δ_{mean} .

Ensemble Convergence. Averaging across multiple random partitions reduces variance and improves anomaly detection reliability.

Proposition 4.2 (Score Variance Reduction). *Let $s^{(k)}(\mathbf{x})$ denote the anomaly score of point \mathbf{x} in the k -th partition. Assuming scores across partitions are independent with variance σ^2 , the variance of the ensemble score $f(\mathbf{x}) = \frac{1}{t} \sum_{k=1}^t s^{(k)}(\mathbf{x})$ is:*

$$\text{Var}[f(\mathbf{x})] = \frac{\sigma^2}{t} \quad (9)$$

Thus, increasing ensemble size t reduces score variance by a factor of $1/t$.

This variance reduction ensures that genuine anomalies, which consistently receive high scores across partitions, are reliably distinguished from normal points whose scores fluctuate randomly.

Separation Between Anomalies and Normal Points. We analyze the expected score difference between anomalies and normal points.

Proposition 4.3 (Expected Score Separation). *Consider a global anomaly \mathbf{x}_g residing in a sparse region with density ρ_{sparse} and a normal point \mathbf{x}_{nor} in a dense region with density ρ_{dense} where $\rho_{\text{sparse}} \ll \rho_{\text{dense}}$. Anomalies tend to: 1) Reside in sparse regions where cells are large; 2) Lie at cell boundaries, far from anchors. The expected cell mean distances satisfy:*

$$\mathbb{E}[\delta_{\text{mean}}(\mathbf{x}_g)] \propto \rho_{\text{sparse}}^{-1/d} \gg \rho_{\text{dense}}^{-1/d} \propto \mathbb{E}[\delta_{\text{mean}}(\mathbf{x}_{\text{nor}})] \quad (10)$$

where d is the feature dimensionality. Combined with the relative position term, anomalies receive significantly higher scores.

This proposition formalizes the intuition that sparse regions amplify anomaly scores through the δ_{mean} weighting factor, creating clear separation between anomalous and normal instances.

These theoretical properties collectively explain SVEAD's effectiveness: random sampling provides density adaptation (Proposition 4.1), ensemble averaging reduces variance (Proposition 4.2) and the dual-factor scoring creates clear separation between anomalies and normal points (Proposition 4.3).

4.4. Algorithm and Complexity Analysis

Algorithm Description. Algorithm 1 presents the complete procedure of SVEAD. The algorithm consists of two phases:

Algorithm 1 SVEAD

Input: Dataset $\mathcal{X} = \{\mathbf{x}_1, \dots, \mathbf{x}_n\}$, anchor count m , ensemble size t

Output: Anomaly scores $\{f(\mathbf{x}_1), \dots, f(\mathbf{x}_n)\}$

```

1: for  $k = 1$  to  $t$  do
2:   Sample anchor set  $\mathcal{A}^{(k)} = \{a_1^{(k)}, \dots, a_m^{(k)}\}$  uniformly from  $\mathcal{X}$ 
3:   for each  $\mathbf{x}_i \in \mathcal{X}$  do
4:      $j^* \leftarrow \arg \min_{j \in [m]} \|\mathbf{x}_i - a_j^{(k)}\|$ 
5:     Assign  $\mathbf{x}_i$  to cell  $C_{j^*}^{(k)}$ 
6:   end for
7:   for each cell  $C_j^{(k)}$  do
8:      $\delta_{\text{max}}^{(k,j)} \leftarrow \max_{\mathbf{x} \in C_j^{(k)}} \|\mathbf{x} - a_j^{(k)}\|$ 
9:      $\delta_{\text{mean}}^{(k,j)} \leftarrow \frac{1}{|C_j^{(k)}|} \sum_{\mathbf{x} \in C_j^{(k)}} \|\mathbf{x} - a_j^{(k)}\|$ 
10:    end for
11:  end for
12:  for each  $\mathbf{x}_i \in \mathcal{X}$  do
13:    Initialize  $f(\mathbf{x}_i) \leftarrow 0$ 
14:    for  $k = 1$  to  $t$  do
15:      Let  $j^*$  be the cell index where  $\mathbf{x}_i \in C_{j^*}^{(k)}$ 
16:       $\delta \leftarrow \|\mathbf{x}_i - a_{j^*}^{(k)}\|$ 
17:       $s^{(k)}(\mathbf{x}_i) \leftarrow \frac{\delta}{\delta_{\text{max}}^{(k,j^*)}} \cdot \delta_{\text{mean}}^{(k,j^*)}$ 
18:       $f(\mathbf{x}_i) \leftarrow f(\mathbf{x}_i) + s^{(k)}(\mathbf{x}_i)$ 
19:    end for
20:     $f(\mathbf{x}_i) \leftarrow f(\mathbf{x}_i)/t$ 
21:  end for
Output:  $\{f(\mathbf{x}_1), \dots, f(\mathbf{x}_n)\}$ 

```

ensemble construction and anomaly scoring. In the construction phase (lines 1-10), we generate t random partitions. For each partition, we sample m anchors uniformly from the dataset and assign each point to its nearest anchor, computing cell statistics including maximum and mean distances. In the scoring phase (lines 11-18), we iterate through all points and partitions, computing within-cell scores using the dual-factor formula and averaging across partitions to obtain final anomaly scores.

Time Complexity. We analyze the computational cost for each algorithmic component:

Partition construction (lines 1-10): Sampling m anchors requires $O(m)$ time. For each of n points, finding the nearest anchor among m candidates requires $O(md)$ operations where d is the feature dimensionality, taking $O(nmd)$ in total. Computing cell statistics requires checking each of n points for each of m cells, taking $O(mn)$ time. Constructing one partition thus requires $O(nmd)$, and building t partitions costs $O(nmdt)$.

Score computation (lines 11-19): For each point and each

partition, computing the within-cell score requires $O(d)$ operations for distance calculation. Processing all points across all partitions requires $O(ndt)$ operations.

The total time complexity is $O(nmdt) + O(ndt) = O(nmdt)$, which simplifies to $O(mnt)$ when d is treated as a constant or is small relative to n . Since $m \ll n$ in practice, this scales **linearly** with dataset size.

Space Complexity. The algorithm stores anchor sets across t partitions requiring $O(tmd)$ space, and cell statistics (δ_{\max} and δ_{mean}) for m cells per partition requiring $O(tm)$ space. The total space complexity is $O(tmd + tm) = O(tmd)$, which simplifies to $O(tm)$ when d is constant. Excluding the input dataset itself, the algorithm’s memory footprint is $O(tm)$, where t and m are constant hyperparameter, thus SVEAD’s space complexity is **constant**.

5. Experiments

This section conducts a comprehensive evaluation with the existing state-of-the-art methods to empirically verify the effectiveness and efficiency of SVEAD. Our evaluation covers a wide range of datasets, including synthetic datasets with different anomaly types and 45 real-world datasets.

5.1. Experimental Setup

Datasets. We evaluate SVEAD on 45 publicly available benchmark datasets widely used in anomaly detection from ADBench (Han et al., 2022). These datasets span diverse domains including medical diagnosis, network security, image recognition, and industrial monitoring, with varying characteristics in terms of dimensionality (ranging from 3 to 1,555 features), sample size (from 80 to 619,326 instances), and anomaly ratio (from 0.17% to 34.99%). The complete list and statistics of datasets are provided in the appendix.

Baseline Methods. We compare SVEAD against 12 state-of-the-art anomaly detection methods spanning different paradigms: traditional methods including LOF (Breunig et al., 2000), Isolation Forest (Liu et al., 2008), iNNE (Bandaragoda et al., 2018), IDK (Ting et al., 2020), ECOD (Li et al., 2022), and COPOD (Li et al., 2020); deep learning methods including DeepSVDD (Ruff et al., 2018), Autoencoder (AE), LUNAR (Goodge et al., 2022), DIF (Xu et al., 2023a), SLAD (Xu et al., 2023b), and DTE (Livernoche et al., 2024). Most algorithms are implemented from the PyOD library (Zhao et al., 2019), while SLAD and DTE are obtained from their official repositories.

Evaluation Metrics. We adopt Area Under the Receiver Operating Characteristic curve (AUC-ROC) and Area Under the Precision-Recall curve (AUC-PR) in the experiment. For each dataset and method, we repeat experiments 5 times and report the mean performance.

Parameter Settings. For fair comparison, we conduct grid search for methods with tunable parameters. LOF’s neighborhood size k is searched over $\{5, 10, 20, 40\}$. For Isolation Forest, iNNE, IDK, and SVEAD, the number of sample points is searched over $\{2^1, 2^2, \dots, 2^8\}$, with ensemble size fixed at 100. ECOD and COPOD are parameter-free and use default settings. Deep learning methods employ default hyperparameters reported in their original papers due to their extensive parameter spaces.

5.2. Overall Performance and Statistical Analysis

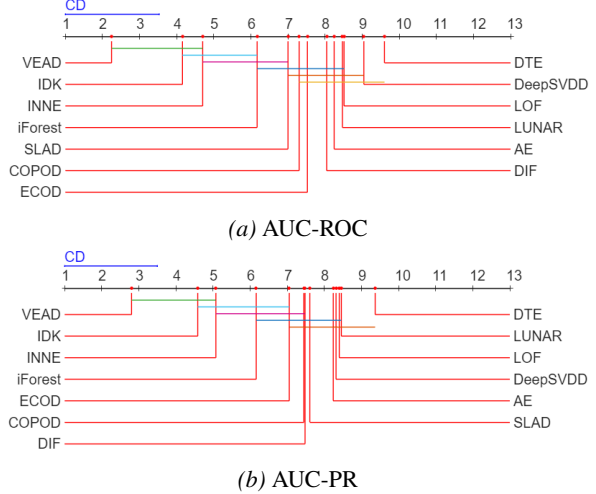
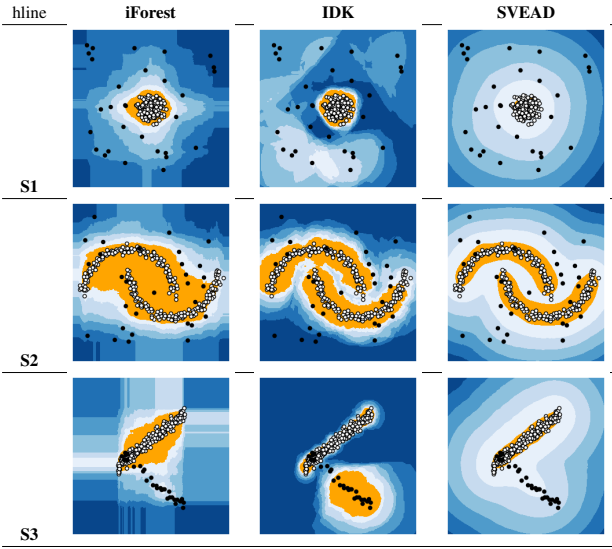


Figure 3. Friedman-Nemenyi test for anomaly detectors at significance level 0.1. If two algorithms are connected by a CD (critical difference) line, there is no significant difference between them.

SVEAD achieves the highest average performance on both AUC-ROC and AUC-PR. Beyond average performance, we conduct rigorous statistical testing to assess whether SVEAD’s improvements are significant. Figure 4 shows Friedman-Nemenyi test results, the critical difference (CD) diagrams reveal that SVEAD achieves the best rank among all methods on both AUC-ROC and AUC-PR metrics. Notably, SVEAD’s rank is significantly better than traditional distance-based methods and most deep learning methods, demonstrating that the geometric partitioning approach combined with dual-factor scoring provides substantial advantages over existing paradigms.

Performance on Different Anomaly Types. To assess SVEAD’s ability to detect diverse anomaly patterns, we construct three synthetic datasets representing canonical anomaly types: global, local and dependency anomalies. Table 2 visualizes detection results using heatmaps, where darker colors indicate higher anomaly scores. The results demonstrate SVEAD’s versatility across anomaly types. On global anomalies, SVEAD, IDK, and Isolation Forest all successfully identify anomalies in sparse regions, confirming that geometric methods handle globally isolated points effec-

Table 2. Performance comparison of iForest and IDK on global (S1), local (S2) and dependency anomaly (S3).



tively. On local anomalies, SVEAD produces significantly sharper boundaries around local deviations compared to IDK, while Isolation Forest struggles due to its axis-aligned partitioning bias. On dependency anomalies, SVEAD captures the anomalous structure more accurately than both baselines.

5.3. Sensitivity and Scalability Analysis

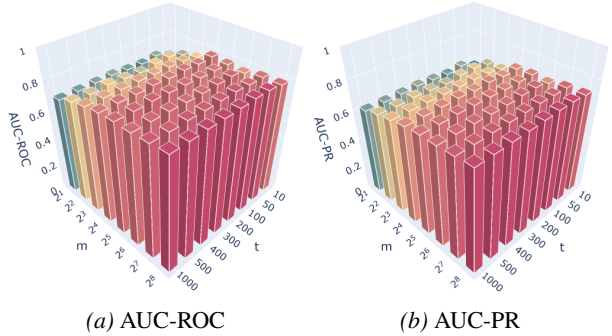


Figure 4. The AUC-ROC and AUC-PR performance with different values of m and t .

Sensitivity Analysis: We investigate SVEAD’s sensitivity to two key hyperparameters: the number of sampled anchors m per partition and the ensemble size t . Figure 4 shows AUC-ROC and AUC-PR performance across `magic_gamma` datasets. SVEAD shows sensitivity to the number of anchor points (m), as this directly determines the granularity of local region partitioning and affects the density adaptation mechanism through Voronoi cell formation. Larger m values create finer partitions that capture more localized density variations, while smaller values may

overlook subtle anomalies in complex data structures. In contrast, ensemble size (t) demonstrates robustness due to variance reduction from ensemble averaging. The stochastic sampling of anchor points introduces variability across individual partitions, but this variance is effectively stabilized through aggregation, making the algorithm relatively insensitive to t .

Scalability Analysis: Figure 5 compares the runtime of SVEAD with the two most competitive algorithms iNNE and IDK. Although all three methods have linear time complexity, SVEAD still demonstrates several-fold faster execution, requiring less than 10 seconds to process 500,000 data points.

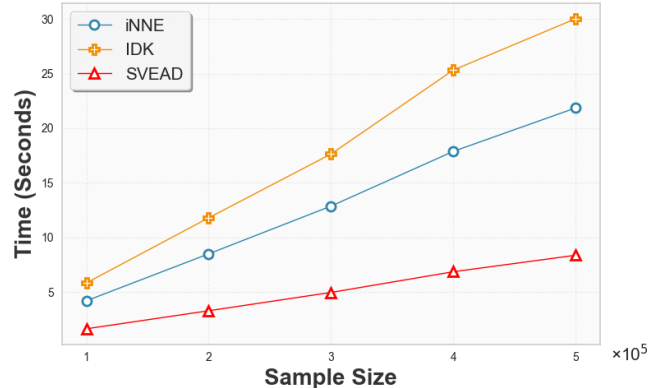


Figure 5. The runtime comparison on `donors` dataset.

6. Conclusion

We propose SVEAD that leverages stochastic Voronoi diagram and ensemble averaging to identify anomalies across diverse data distributions. The core contribution lies in recognizing that local anomalies, though indistinguishable under global analysis, become conspicuous when the data space is decomposed into restricted spatial regions. By randomly sampling anchors to induce Voronoi partitions and scoring points through normalized cell-relative distances weighted by local scale, SVEAD achieves automatic density adaptation without explicit parameter tuning or k-NN computations. Theoretical analysis establishes that random anchor sampling provides density-adaptive partitioning, ensemble averaging reduces variance and ensures robustness, and the dual-factor scoring mechanism creates clear separation between anomalous and normal instances. Extensive experiments on 45 benchmark datasets demonstrate that SVEAD achieves state-of-the-art performance with linear time complexity, outperforming 12 baselines. The method’s effectiveness across global, local, and dependency anomaly types, combined with its computational efficiency, makes it a practical solution for large-scale anomaly detection applications.

References

Angiulli, F. and Pizzuti, C. Fast outlier detection in high dimensional spaces. In *European conference on principles of data mining and knowledge discovery*, pp. 15–27. Springer, 2002.

Bandaragoda, T. R., Ting, K. M., Albrecht, D., Liu, F. T., Zhu, Y., and Wells, J. R. Isolation-based anomaly detection using nearest-neighbor ensembles. *Computational Intelligence*, 34(4):968–998, 2018.

Breunig, M. M., Kriegel, H.-P., Ng, R. T., and Sander, J. Lof: identifying density-based local outliers. In *Proceedings of the 2000 ACM SIGMOD international conference on Management of data*, pp. 93–104, 2000.

Cao, Y., Ma, Y., Tang, X., Rasheed, R. A., and Li, H. X. A data-driven framework for identifying abnormal status in natural gas wells. In *International Conference on Advanced Data Mining and Applications*, pp. 105–119. Springer, 2024a.

Cao, Y., Ma, Y., Zhu, Y., and Ting, K. M. Revisiting streaming anomaly detection: benchmark and evaluation. *Artificial Intelligence Review*, 58(1):8, 2024b.

Cao, Y., Pokhrel, S. R., Zhu, Y., Doss, R., and Li, G. Automation and orchestration of zero trust architecture: Potential solutions and challenges. *Machine Intelligence Research*, 21(2):294–317, 2024c.

Cao, Y., Zhu, Y., Ting, K. M., Salim, F. D., Li, H. X., Yang, L., and Li, G. Detecting change intervals with isolation distributional kernel. *Journal of Artificial Intelligence Research*, 79:273–306, 2024d.

Cao, Y., Xiang, H., Zhang, H., Zhu, Y., and Ting, K. M. Anomaly detection based on isolation mechanisms: A survey. *Machine Intelligence Research*, pp. 1–17, 2025a.

Cao, Y., Yang, S., Yang, Y., Qi, L., and Liu, M. Text anomaly detection with simplified isolation kernel. In Christodoulopoulos, C., Chakraborty, T., Rose, C., and Peng, V. (eds.), *Findings of the Association for Computational Linguistics: EMNLP 2025*, pp. 12702–12713, Suzhou, China, November 2025b. Association for Computational Linguistics. ISBN 979-8-89176-335-7. doi: 10.18653/v1/2025.findings-emnlp.680. URL <https://aclanthology.org/2025.findings-emnlp.680/>.

Chandola, V., Banerjee, A., and Kumar, V. Anomaly detection: A survey. *ACM computing surveys (CSUR)*, 41(3):1–58, 2009.

Goodge, A., Hooi, B., Ng, S.-K., and Ng, W. S. Lunar: Unifying local outlier detection methods via graph neural networks. In *Proceedings of the AAAI Conference on Artificial Intelligence*, volume 36, pp. 6737–6745, 2022.

Han, S., Hu, X., Huang, H., Jiang, M., and Zhao, Y. Ad-bench: Anomaly detection benchmark. *Advances in neural information processing systems*, 35:32142–32159, 2022.

Li, Z., Zhao, Y., Botta, N., Ionescu, C., and Hu, X. Copod: copula-based outlier detection. In *2020 IEEE international conference on data mining (ICDM)*, pp. 1118–1123. IEEE, 2020.

Li, Z., Zhao, Y., Hu, X., Botta, N., Ionescu, C., and Chen, G. H. Ecod: Unsupervised outlier detection using empirical cumulative distribution functions. *IEEE Transactions on Knowledge and Data Engineering*, 35(12):12181–12193, 2022.

Liu, F. T., Ting, K. M., and Zhou, Z.-H. Isolation forest. In *2008 eighth ieee international conference on data mining*, pp. 413–422. IEEE, 2008.

Liu, J., Xie, G., Wang, J., Li, S., Wang, C., Zheng, F., and Jin, Y. Deep industrial image anomaly detection: A survey. *Machine Intelligence Research*, 21(1):104–135, 2024.

Livernoche, V., Jain, V., Hezaveh, Y., and Ravanbakhsh, S. On diffusion modeling for anomaly detection. In *The Twelfth International Conference on Learning Representations*, 2024.

Pang, G., Shen, C., Cao, L., and Hengel, A. V. D. Deep learning for anomaly detection: A review. *ACM computing surveys (CSUR)*, 54(2):1–38, 2021.

Ramaswamy, S., Rastogi, R., and Shim, K. Efficient algorithms for mining outliers from large data sets. In *Proceedings of the 2000 ACM SIGMOD international conference on Management of data*, pp. 427–438, 2000.

Ruff, L., Vandermeulen, R., Goernitz, N., Deecke, L., Sidiqui, S. A., Binder, A., Müller, E., and Kloft, M. Deep one-class classification. In *International conference on machine learning*, pp. 4393–4402. PMLR, 2018.

Ting, K. M., Xu, B.-C., Washio, T., and Zhou, Z.-H. Isolation distributional kernel: A new tool for kernel based anomaly detection. In *Proceedings of the 26th ACM SIGKDD international conference on knowledge discovery & data mining*, pp. 198–206, 2020.

Ting, K. M., Xu, B.-C., Washio, T., and Zhou, Z.-H. Isolation distributional kernel: A new tool for point and group anomaly detections. *IEEE Transactions on Knowledge and Data Engineering*, 35(3):2697–2710, 2021.

Ting, K. M., Liu, Z., Gong, L., Zhang, H., and Zhu, Y. A new distributional treatment for time series anomaly detection. *The VLDB Journal*, 33(3):753–780, 2024.

Xu, H., Pang, G., Wang, Y., and Wang, Y. Deep isolation forest for anomaly detection. *IEEE Transactions on Knowledge and Data Engineering*, 35(12):12591–12604, 2023a.

Xu, H., Wang, Y., Wei, J., Jian, S., Li, Y., and Liu, N. Fascinating supervisory signals and where to find them: Deep anomaly detection with scale learning. In *International Conference on Machine Learning*, pp. 38655–38673. PMLR, 2023b.

Xu, Y., Ma, Y., Zhang, K., Yang, Z., and Ting, K. M. Idk-s: Incremental distributional kernel for streaming anomaly detection. *arXiv preprint arXiv:2512.05531*, 2025.

Zhao, Y., Nasrullah, Z., and Li, Z. Pyod: A python toolbox for scalable outlier detection. *Journal of Machine Learning Research*, 20(96):1–7, 2019. URL <http://jmlr.org/papers/v20/19-011.html>.

A. Full result.

Table 3. Results in term of AUC-ROC

Data	LOF	iForest	iNNE	IDK	ECOD	COPOD	D.SVDD	AE	LUNAR	DIF	SLAD	DTE	VEAD
ALOI	0.7668	0.5392	0.6506	0.6009	0.5305	0.5152	0.5395	0.5589	<u>0.7058</u>	0.5490	0.5258	0.5256	0.6046
annthyroid	0.7392	0.8611	0.7542	0.7119	0.7887	0.7760	0.6522	0.7341	0.7303	0.6758	<u>0.8696</u>	0.5593	0.9427
backdoor	0.7469	0.7355	0.8773	0.8626	0.8462	0.7893	0.8934	0.8900	0.5234	<u>0.9215</u>	0.9098	0.8709	0.9216
breastw	0.4687	0.9946	0.9843	<u>0.9949</u>	0.9914	0.9944	0.9152	0.9635	0.9681	0.7989	0.6033	0.8699	0.9956
campaign	0.5982	0.7085	0.6818	0.6955	0.7697	<u>0.7830</u>	0.6886	0.7548	0.6498	0.6779	0.7148	0.7099	0.8319
cardio	0.6179	0.9260	<u>0.9447</u>	0.9531	0.9350	0.9219	0.9001	0.7507	0.6089	0.9281	0.4975	0.7651	0.9339
Cardio2	0.6271	0.6914	<u>0.7907</u>	0.7701	0.7853	0.6629	0.6893	0.5644	0.5252	0.6211	0.6765	0.4703	0.8470
celeba	0.4786	0.7188	0.7429	<u>0.7762</u>	0.7572	0.7508	0.7397	0.7253	0.5624	0.6493	0.7436	0.8034	0.7591
census	0.5761	0.6138	0.5755	0.6202	0.6595	<u>0.6740</u>	0.6442	0.6722	0.6445	0.5784	0.5825	0.5448	0.6869
donors	0.6153	0.8476	0.8193	0.8777	0.8885	0.8151	0.8016	0.8325	0.6066	0.6873	0.5485	0.8072	0.879
fault	0.5973	0.5608	0.6146	0.6912	0.4687	0.4553	0.5170	0.6489	<u>0.7202</u>	0.6889	0.7131	0.5873	0.7543
fraud	0.4899	0.9518	0.9575	<u>0.9525</u>	0.9496	0.9475	0.9337	0.9431	0.9276	0.9503	0.9401	0.9405	0.9473
glass	0.8466	0.7883	0.8246	0.8481	0.7046	0.7550	0.6249	0.8108	0.8502	0.8507	0.8900	0.6133	<u>0.8697</u>
Hepatitis	0.5890	0.7201	0.5747	0.5711	0.7394	0.8037	0.6429	0.7463	0.5931	0.7137	0.5844	0.3823	<u>0.7897</u>
http	0.4392	0.9998	0.9968	0.9987	0.9786	0.9915	0.9972	0.9747	0.2614	0.9933	0.9992	0.9963	1.0000
InternetADs	0.6470	0.6828	<u>0.6954</u>	0.6891	0.6770	0.6764	0.6045	0.5593	0.6960	0.5522	0.6158	0.5901	0.6935
Ionosphere	0.8944	0.8503	0.8910	0.8861	0.7284	0.7895	0.7246	0.8909	0.9182	0.9015	0.9414	0.8869	<u>0.9315</u>
landsat	0.5466	0.4666	0.6148	0.6992	0.3678	0.4215	0.3918	0.5107	0.5714	0.5583	<u>0.6667</u>	0.5242	0.6021
letter	0.9131	0.6179	<u>0.9213</u>	0.9216	0.5326	0.5032	0.5167	0.8365	0.8880	0.6474	0.7394	0.7774	0.8949
Lymphography	0.9906	0.9991	0.9948	0.9901	0.9953	0.9965	0.9862	0.9812	0.9596	0.9202	0.9636	0.9688	<u>0.9986</u>
magic.gamma	0.7110	0.7240	0.7491	0.7584	0.6382	0.6812	0.6282	0.7409	<u>0.8192</u>	0.7587	0.6243	0.7590	0.8241
mammography	0.7351	0.8659	0.8659	0.8719	0.9062	<u>0.9053</u>	0.8819	0.8351	0.8390	0.7450	0.6929	0.8265	0.8749
mnist	0.7133	0.8043	0.8384	0.8370	0.7463	0.7739	0.7951	0.8369	0.7416	<u>0.8699</u>	0.9302	0.5424	0.8664
musk	0.4912	<u>0.9997</u>	1.0000	1.0000	0.9559	0.9463	0.9466	0.8562	0.3118	0.9819	0.8706	0.5599	1.0000
optdigits	0.6660	<u>0.7352</u>	0.8338	0.9019	0.6045	0.6824	0.4551	0.4781	0.4243	0.5670	0.5751	0.5000	0.7035
PageBlocks	0.8328	0.8974	0.8958	0.8561	<u>0.9139</u>	0.8754	0.9067	0.8789	0.7631	0.8811	0.9109	0.4860	0.9533
pendigits	0.5230	0.9542	0.9291	0.9581	0.9274	0.9048	0.7582	0.8416	0.6938	0.9440	0.9624	0.8864	<u>0.9603</u>
Pima	0.5995	<u>0.6957</u>	0.6493	0.6389	0.5944	0.6540	0.6773	0.6278	0.6886	0.6122	0.4812	0.4455	0.7311
satellite	0.5637	<u>0.6996</u>	0.7465	0.8046	0.5830	0.6335	0.6111	0.6658	0.6380	0.7395	0.6270	0.5832	<u>0.7905</u>
satimage-2	0.5765	0.9948	<u>0.9978</u>	0.9975	0.9649	0.9745	0.964	0.9033	0.8993	0.9969	0.9615	0.496	0.9988
shuttle	0.5819	0.9972	0.9942	0.9934	0.9929	0.9945	0.9883	0.9331	0.6725	0.9672	0.9033	0.5	<u>0.9951</u>
skin	0.5537	0.6713	0.7535	0.8075	0.4888	0.4711	0.5333	0.6827	0.7156	0.6688	0.8390	0.7662	0.7773
smtp	0.9270	0.9173	0.9460	0.9565	0.8801	0.9120	0.8444	0.8987	0.9215	0.8521	0.8122	0.9157	0.9296
SpamBase	0.5079	0.6981	<u>0.7138</u>	<u>0.7245</u>	0.6556	0.6879	0.5589	0.5533	0.5205	0.3901	0.3985	0.5629	0.7376
speech	0.6494	0.4828	0.6730	0.7389	0.4697	0.4911	0.5035	0.4751	0.4970	0.4896	0.5463	0.5270	<u>0.6919</u>
Stamps	0.7076	<u>0.9253</u>	0.8900	0.9114	0.8761	0.9302	0.8422	0.8277	0.8456	0.8589	0.8354	0.8320	0.9064
thyroid	0.9287	<u>0.9872</u>	0.9566	0.9577	0.9771	0.9393	0.9295	0.9238	0.9361	0.9595	0.9654	0.9029	0.9915
vertebral	0.5298	0.3770	0.5640	0.5579	0.4200	0.3349	0.3413	0.4660	0.4001	0.4972	0.4176	<u>0.6728</u>	0.7345
vowels	0.9434	0.7736	0.9392	<u>0.9542</u>	0.5929	0.4958	0.6164	0.9385	0.9220	0.8116	0.9456	<u>0.9334</u>	0.9802
Waveform	0.7632	0.7147	0.8410	<u>0.8679</u>	0.6035	0.7339	0.5648	0.6085	0.7300	0.7255	0.8842	0.6316	0.8345
WBC	0.9685	<u>0.9963</u>	0.9955	0.9947	0.9948	0.9948	0.9924	0.9587	0.9630	0.8130	0.8606	0.5716	0.9975
WDBC	0.9989	0.9888	<u>0.9987</u>	0.9990	0.9706	0.9941	0.9842	0.9300	0.9593	0.7087	0.9986	0.5831	0.9992
Wilt	0.7750	0.4625	<u>0.7683</u>	0.7572	0.3940	0.3447	0.3449	0.5634	0.5159	0.3788	0.4915	0.4689	0.7177
wine	0.9992	0.8304	0.9988	0.9991	0.7328	0.8672	0.7368	0.7613	0.3753	0.5139	0.9210	0.3820	0.9987
WPBC	0.5185	0.5075	0.5124	0.5167	0.4813	0.5233	0.4658	0.4753	0.4947	0.4690	0.5359	0.4011	0.5414
Average	0.6879	0.7772	0.8213	0.8327	0.7435	0.7504	0.7172	0.7558	0.6933	0.7348	0.7493	0.6651	0.8538

Table 4. Results in term of AUC-PRC

Data	LOF	iforest	iNNE	IDK	ECOD	COPOD	D.SVDD	AE	LUNAR	DIF	SLAD	DTE	VEAD
ALOI	0.1033	0.0337	0.0894	0.0623	0.0329	0.0313	0.0369	0.0404	0.0906	0.0427	0.0444	0.0436	0.0683
annthyroid	0.2053	0.3963	0.2043	0.2001	0.2697	0.1733	0.1766	0.2178	0.1834	0.2196	<u>0.4167</u>	0.1142	0.6050
backdoor	0.2075	0.0459	0.1310	0.1059	0.0923	0.0685	<u>0.5821</u>	0.4967	0.0481	0.4099	0.5390	0.3900	0.5925
breastw	0.3064	0.9893	0.9618	<u>0.9900</u>	0.9839	0.9886	0.9189	0.9010	0.9192	0.4900	0.5509	0.6715	0.9914
campaign	0.1344	0.2955	0.2181	0.2160	<u>0.3546</u>	0.3686	0.2470	0.2470	0.1932	0.2441	0.2888	0.2613	0.3267
cardio	0.1729	0.5861	0.5684	0.6381	0.5674	0.5776	0.5231	0.3038	0.2066	0.5909	0.1653	0.2948	0.5356
Cardio2	0.3196	0.4348	0.4645	0.4310	<u>0.5054</u>	0.4001	0.4053	0.3133	0.2784	0.4171	0.3426	0.2378	0.5567
celeba	0.0202	0.0694	0.0805	0.0867	0.0969	<u>0.0944</u>	0.0817	0.0542	0.0262	0.0463	0.0461	0.0677	0.0835
census	0.0750	0.0742	0.0692	0.0736	0.0840	<u>0.0877</u>	0.0834	0.0909	0.0818	0.0672	0.0682	0.0657	<u>0.0882</u>
cover	0.0175	0.0459	0.3059	<u>0.2988</u>	0.1072	0.0658	0.0606	0.0700	0.0376	0.2025	0.0135	0.0189	0.0569
donors	0.1039	0.1947	0.1571	<u>0.2066</u>	0.2641	<u>0.2082</u>	0.1603	0.1686	0.1017	0.0825	0.0597	0.1414	0.2057
fault	0.4020	0.4038	0.4693	0.5062	0.3257	0.3127	0.3685	0.4824	<u>0.5365</u>	0.5361	0.5291	0.4211	0.5664
fraud	0.0016	0.2010	0.1541	0.1147	0.2167	0.2431	0.1158	0.1495	0.1075	<u>0.3700</u>	0.1274	0.2925	0.4176
glass	0.2539	0.1150	0.1535	0.1433	0.1859	0.1085	0.1067	0.1655	0.1796	<u>0.2347</u>	0.1817	0.0793	0.2089
Hepatitis	0.2640	0.2736	0.2215	0.2310	0.2934	<u>0.3941</u>	0.2785	0.3264	0.1963	0.2971	0.1891	0.1486	0.4190
http	0.0070	<u>0.9513</u>	0.6378	0.7092	0.1453	0.3018	0.5802	0.1246	0.0004	0.3505	0.8236	0.5517	0.9985
InternetADs	0.4070	0.4655	<u>0.5203</u>	0.5222	0.5089	0.5077	0.2697	0.2092	0.3879	0.2047	0.2688	0.2914	0.3861
Ionosphere	0.8645	0.8013	0.8798	0.8611	0.6461	<u>0.6697</u>	0.5959	0.8619	0.9186	0.8722	0.9011	0.8536	<u>0.9173</u>
landsat	0.2516	0.1960	0.2714	0.3332	0.1635	0.1758	0.1922	0.2231	0.2493	0.2514	<u>0.3021</u>	0.2153	0.2491
letter	0.6071	0.0850	0.5722	<u>0.5754</u>	0.0757	0.0730	0.0690	0.2795	0.3810	0.1114	0.1628	0.3104	0.3618
Lymphography	0.8215	0.9813	0.9001	<u>0.7510</u>	0.8972	0.9151	0.7839	0.7306	0.8485	0.4422	0.5099	0.4774	<u>0.9704</u>
magic.gamma	0.5560	0.6399	0.6478	0.6318	0.5335	0.5881	0.5538	0.6399	<u>0.7492</u>	0.6761	0.4740	0.6607	0.7544
mammography	0.1160	0.2163	0.1795	0.1892	0.4360	<u>0.4300</u>	0.2149	0.1171	0.1486	0.1213	0.0567	0.1829	0.1869
mnist	0.2426	0.2705	0.3370	0.3270	0.1780	0.2140	0.3434	0.3610	0.2980	<u>0.4038</u>	0.5749	0.1188	0.3836
musk	0.1283	<u>0.9902</u>	1.0000	1.0000	0.4918	0.3433	0.6828	0.4097	0.0453	0.7202	0.2283	0.0521	1.0000
optdigits	0.0545	0.0544	<u>0.0810</u>	0.1357	0.0337	0.0422	0.0256	0.0255	0.0264	0.0323	0.0322	0.0288	0.0473
PageBlocks	0.4875	0.4655	0.5501	<u>0.5667</u>	0.5199	0.3710	0.5664	0.3944	0.3655	0.5064	0.4937	0.1825	0.6769
pendigits	0.0486	0.2974	0.2262	<u>0.3056</u>	0.2656	0.1824	0.1157	0.0797	0.0544	0.2441	0.3475	0.0987	0.2837
Pima	0.4324	0.5422	0.4970	0.4912	0.4642	0.5054	0.5126	0.4458	0.5050	0.4124	0.3633	0.3674	0.5334
satellite	0.3916	0.6733	0.6194	<u>0.6851</u>	0.5261	0.5706	0.5633	0.5504	0.4785	0.6795	0.4181	0.3964	0.7126
satimage-2	0.0634	0.9348	<u>0.9654</u>	0.8279	0.6597	0.7933	0.6428	0.2985	0.1578	0.7737	0.3576	0.0120	0.9723
shuttle	0.1275	0.9798	0.8840	0.8511	0.9043	<u>0.9608</u>	0.9059	0.6271	0.1794	0.5897	0.3544	0.0715	0.9005
skin	0.2353	0.2546	0.3166	<u>0.3747</u>	0.1821	0.1783	0.2045	0.2621	0.2911	0.2551	0.4854	0.3236	0.3367
smtp	0.0272	0.0775	0.3888	0.2803	<u>0.5073</u>	0.0041	0.2267	0.0035	0.0582	0.4560	0.0224	0.3828	0.5337
SpamBase	0.3952	0.5631	0.6195	<u>0.6299</u>	0.5183	0.5438	0.4181	0.4150	0.4160	0.3331	0.3436	0.4964	0.6338
speech	0.0703	0.0188	0.1180	<u>0.1155</u>	0.0196	0.0193	0.0189	0.0186	0.0197	0.0195	0.0194	0.0200	0.0820
Stamps	0.2018	<u>0.3753</u>	0.3268	0.3716	0.3142	0.3961	0.2767	0.3049	0.3152	0.2737	0.2954	0.2569	0.3594
thyroid	0.2073	<u>0.6536</u>	0.3110	0.3507	0.4678	0.1789	0.2859	0.3636	0.2516	0.4438	0.5781	0.2177	0.7622
vertebral	0.1318	<u>0.0967</u>	0.1489	0.1673	0.1072	0.0903	0.0918	0.1169	0.0999	0.1248	0.1022	0.2043	0.2088
vowels	0.3325	0.1619	0.3763	0.5163	0.0814	0.0341	0.0998	<u>0.5506</u>	0.5272	0.1643	0.3595	0.3500	0.6643
Waveform	0.1236	0.0549	0.1311	<u>0.2099</u>	0.0405	0.0559	0.0372	0.0489	0.1162	0.0638	0.4494	0.0506	0.1076
WBC	0.5045	<u>0.9388</u>	0.9198	0.9152	0.9038	0.9038	0.9040	0.5680	0.7120	0.1342	0.3530	0.0769	0.9642
WDBC	0.9573	0.6515	0.9472	<u>0.9657</u>	0.5053	0.8037	0.5343	0.2650	0.3963	0.0527	0.9558	0.5259	0.9711
Wilt	0.1130	0.0448	0.1115	0.1231	0.0417	0.0370	0.0373	0.0559	0.0498	0.0389	0.0533	0.0518	0.0839
wine	0.9909	0.3014	0.9829	0.9851	0.1907	0.3612	0.2646	0.1579	0.0655	0.0869	0.4137	0.0843	0.9854
WPBC	0.2316	0.2334	0.2316	0.2328	0.2178	0.2378	0.2192	0.2166	0.2251	0.2190	0.2603	0.2048	0.2479
Average	0.2765	0.3941	0.4336	0.4414	0.3462	0.3394	0.3344	0.2990	0.2723	0.3111	0.3244	0.2471	0.5000